

# Leveraging Variational Autoencoders for Parameterized MMSE Channel Estimation

Michael Baur, *Graduate Student Member, IEEE*, Benedikt Fesl, *Graduate Student Member, IEEE*, and Wolfgang Utschick, *Fellow, IEEE*

**Abstract**—In this manuscript, we propose to utilize the generative neural network-based variational autoencoder for channel estimation. The variational autoencoder models the underlying true but unknown channel distribution as a conditional Gaussian distribution in a novel way. The derived channel estimator exploits the internal structure of the variational autoencoder to parameterize an approximation of the mean squared error optimal estimator resulting from the conditional Gaussian channel models. We provide a rigorous analysis under which conditions a variational autoencoder-based estimator is mean squared error optimal. We then present considerations that make the variational autoencoder-based estimator practical and propose three different estimator variants that differ in their access to channel knowledge during the training and evaluation phase. In particular, the proposed estimator variant trained solely on noisy pilot observations is particularly noteworthy as it does not require access to noise-free, ground-truth channel data during training or evaluation. Extensive numerical simulations first analyze the internal behavior of the variational autoencoder-based estimators and then demonstrate excellent channel estimation performance compared to related classical and machine learning-based state-of-the-art channel estimators.

**Index Terms**—Channel estimation, deep learning, variational autoencoder, MMSE estimator, machine learning.

## I. INTRODUCTION

Channel estimation (CE) is crucial to attain the full potential of massive multiple-input multiple-output (MIMO) communications systems [2]. Developing novel CE techniques is, therefore, of ever-evolving interest. Machine learning (ML) and deep learning (DL), in specific, are promising candidates for further improvements of massive MIMO systems [3]. DL-based methods, for example, take into account the characteristics of a communication scenario by training a deep neural network (DNN) based on data from the scenario’s particular radio propagation environment. The DNN can then often leverage the acquired knowledge about the scenario to outperform classical methods in typical tasks such as CE. The outstanding performance of DL-based CE has been demonstrated in many publications, e.g., see [4]–[8]. Two major categories of such methods exist: end-to-end learning and model-based approaches. In end-to-end learning, task-specific DNN architectures and cost functions are designed, which are trained on a large number of training samples [9]. Model-based methods follow a different philosophy. They combine

mathematical models and DL by replacing specific elements in the model with a DNN [10], [11]. The replaced elements are usually the parts of the model that are intricate or impossible to describe analytically. Model-based methods leverage the approximation capabilities of DNNs to learn the unknown parts of the model exclusively. The remainder of the processing scheme is left untouched. Among others, the benefits of model-based methods compared to end-to-end learning lie in their interpretability and reduced requirements for computational resources and training data.

In this work, we want to explore a model-based approach for CE via generative modeling. Generative modeling refers to a class of ML techniques that aim to create or generate new samples which follow the same distribution as the training samples [12]. The goal is to learn the underlying distribution of the data. Among the most prominent generative models are Gaussian mixture models (GMMs) [13, Ch. 9], variational autoencoders (VAEs) [14], [15], generative adversarial networks (GANs) [16], and normalizing flows (NFs) [17]. Prior research demonstrates that generative models offer large CE performance gains compared to related baseline methods. For instance, the authors of [18] use a GMM for CE, and in [19], [20] a GAN is utilized. The generative model-based methods share the property that they aim to learn the channel distribution during the training phase and exploit the extracted a priori information in the subsequent estimation phase.

The related GMM-based channel estimator parameterizes an approximation to the mean squared error (MSE)-optimal conditional mean estimator (CME) [18]. After the successful fitting of the GMM parameters to available channel data representing the particular radio propagation environment, the authors use the GMM for pilot-based CE. It was proved that the proposed GMM-based estimator converges asymptotically to the CME with an increasing number of mixture components. A GMM and a VAE share some properties: both maximize a lower bound to the data log-likelihood and introduce an artificial latent space. The latent space of the GMM is discrete, whereas it is continuous in the case of the VAE. The VAE demonstrates its capabilities in various communications-oriented problems. This includes channel equalization [21]–[23], signal detection [24], device activity detection [25], and channel modeling for a UAV scenario [26]. However, to our knowledge, no approaches in the literature exist that use the VAE for pilot-based CE.

**Contributions:** We propose a VAE-based framework for pilot-based CE, where we model the analytically intractable channel distribution of a radio propagation environment as

Preliminary results have been reported at Asilomar’22 [1].

This work receives funding by the Bavarian Ministry of Economic Affairs, Regional Development and Energy within the project 6G Future Lab Bavaria.

The authors acknowledge the financial support by the Federal Ministry of Education and Research of Germany in the programme of “Souverän. Digital. Vernetzt.”. Joint project 6G-life, project identification number: 16KISK002

conditionally Gaussian (CG) with the help of the VAE. The CG modeled channel distribution combined with a successfully trained VAE allows us to approximate the MSE-optimal estimator. To this end, we use the conditional first and second-order statistical moments at the VAE decoder to parameterize individual linear minimum mean squared error (LMMSE) channel estimators given the latent representation and noisy pilot observation. Furthermore, the individual LMMSE estimators are the MSE-optimal estimators given the latent representation under the framework. We obtain the latent representation for the noisy pilot observation in this context with the help of the VAE encoder. Note that the VAE does not try to learn a direct mapping from a noisy pilot observation to a channel estimate at any point. It instead learns the underlying channel distribution and exploits the structure of the VAE to parameterize an estimator. We provide a rigorous analysis of the theoretical capabilities of the proposed VAE-based channel estimator that backs its strong CE results. Overall, three variants of VAE-based channel estimators are proposed, which differ in the availability of channel knowledge during their training and evaluation operation phase. The so-called VAE-real method we propose is particularly noteworthy as it does not require access to samples of noise-free channel data in either the training or evaluation phases. Our extensive numerical simulations underline the superiority of the proposed VAE-based estimator variants compared to the baseline methods under various system configurations.

Moreover, we provide the following extensions in this manuscript compared to the preliminary results in [1]. The analyses in Sections III-B and III-C enhance the theoretical foundation of the MSE-optimality. We extend the estimator to the more general MIMO case and make the training of the VAE signal-to-noise ratio (SNR)-independent. The latter means that we use a single trained VAE for every SNR value, in opposition to [1], where a different VAE is trained for every SNR value. Finally, the numerical simulations in this manuscript are more extensive and shed light on the internal processes of the VAE in Section VI-A.

The structure of this manuscript is as follows. Section II introduces the system and channel models and the general problem formulation. Section III first provides background information about the VAE. Then, we derive the VAE-based channel estimator followed by a convergence analysis. We discuss practical aspects of the implementation in Section IV, which are the variants of the VAE-based estimators, the specific DNN architecture, and the computational complexity of the estimation. Numerical simulation results are presented in Section VI, and we conclude this manuscript in Section VII.

*Notation:* We denote vector and matrices as lower-case and upper-case bold-faced symbols, respectively. Scalars are non-bold-faced. The norm  $\|\mathbf{b}\|$  represents the Euclidean norm of a vector  $\mathbf{b} \in \mathbb{C}^N$ . The norm  $\|p\|_\infty$  represents the supremum norm of a continuous function  $p$ . Element-wise multiplication is denoted as  $\odot$  and the all-ones vector as  $\mathbf{1}$ . The vectorization  $\text{vec}(\mathbf{G}) \in \mathbb{C}^{g_1 g_2}$  stacks the columns of  $\mathbf{G} \in \mathbb{C}^{g_1 \times g_2}$  into a vector. The kronecker product of two matrices  $\mathbf{B} \in \mathbb{C}^{b_1 \times b_2}$  and  $\mathbf{D} \in \mathbb{C}^{d_1 \times d_2}$  is  $(\mathbf{B} \otimes \mathbf{D}) \in \mathbb{C}^{b_1 d_1 \times b_2 d_2}$ .

## II. SYSTEM AND CHANNEL MODEL

We consider the uplink of a typical MIMO point-to-point system. A base station (BS) equipped with  $N_{\text{rx}}$  antennas receives pilot signals from an  $N_{\text{tx}}$  antenna mobile terminal (MT). In particular, the BS receives noisy pilot observations

$$\mathbf{y}_i = \mathbf{H} \mathbf{x}_i + \mathbf{n}_i, \quad i = 1, \dots, P, \quad (1)$$

of in total  $P$  pilots  $\mathbf{x}_i \in \mathbb{C}^{N_{\text{tx}}}$  as a linear mapping over the channel  $\mathbf{H} \in \mathbb{C}^{N_{\text{rx}} \times N_{\text{tx}}}$  with additive noise  $\mathbf{n}_i \sim \mathcal{N}_{\mathbb{C}}(\mathbf{0}, \Sigma)$ . By arranging the involved vectors as matrices, we can express the model as

$$\mathbf{Y} = \mathbf{H} \mathbf{X} + \mathbf{N} \quad (2)$$

with  $\mathbf{Y} = [\mathbf{y}_1, \dots, \mathbf{y}_P]$ ,  $\mathbf{X} = [\mathbf{x}_1, \dots, \mathbf{x}_P]$ , and  $\mathbf{N} = [\mathbf{n}_1, \dots, \mathbf{n}_P]$ . For our purposes, it is beneficial to vectorize the matrix  $\mathbf{Y}$  to obtain the generic inverse problem

$$\mathbf{y} = \text{vec}(\mathbf{Y}) = \mathbf{A} \mathbf{h} + \mathbf{n} \quad (3)$$

with the observation matrix  $\mathbf{A} = (\mathbf{X}^T \otimes \mathbf{I}_{N_{\text{rx}}})$ , the vectorized channel  $\mathbf{h} = \text{vec}(\mathbf{H}) \in \mathbb{C}^N$  with  $N = N_{\text{rx}} N_{\text{tx}}$ , and  $\mathbf{n} = \text{vec}(\mathbf{N}) \in \mathbb{C}^{N_{\text{rx}} P}$ . Throughout our work, we assume that the BS and MT are both equipped with a uniform linear array (ULA) with half-wavelength spacing. Furthermore, we consider the fully determined case of (3) with  $P = N_{\text{tx}}$  and unitary  $\mathbf{X}$ , which results in a unitary  $\mathbf{A}$ . We do not cover the case of a broad or non-unitary  $\mathbf{A}$ , which includes  $P < N_{\text{tx}}$  and wideband systems, as it exceeds the scope of this manuscript. The authors of [18], [27], [28] offer guidelines on how potential extensions of the proposed estimators can look like since therein the authors extend the related GMM-based estimator to the cases mentioned above. It is reasonable to assume that the proposed VAE-based estimator can be extended likewise, which is part of our future work.

The transmit- and receive-side channel covariance matrix (CCM) of a ULA are Toeplitz structured because of their uniform spacing into a single direction. A valuable feature of Toeplitz CCMs is that they can be asymptotically approximated by circulant matrices for a large number of antennas [29]. Diagonalization of a circulant CCM  $\mathbf{C}$  is possible with the help of the discrete fourier transform (DFT) matrix  $\mathbf{F} \in \mathbb{C}^{M \times M}$ , that is,

$$\mathbf{C} = \mathbf{F}^H \text{diag}(\mathbf{c}) \mathbf{F}, \quad \mathbf{c} \in \mathbb{R}_+^M. \quad (4)$$

The benefit of the circulant approximation property is that (4) allows to invert  $\mathbf{C}$  straightforwardly in  $\mathcal{O}(M \log M)$  time. It also reduces the number of parameters to define a CCM to a positive, real-valued vector  $\mathbf{c}$ . In Section III, we will use the circulant approximation to design channel estimators.

We reported preliminary research results concerning the single-input multiple-output (SIMO) system model in [1]. In this case, the problem in (3) simplifies to

$$\mathbf{y} = \mathbf{h} + \mathbf{n} \quad (5)$$

after decorrelating the single pilot sent from the MT. The matrix  $\mathbf{A}$  in (3) becomes an identity matrix. If we multiply (2) with the unitary  $\mathbf{X}^H$  from the right, we end up with

$$\mathbf{Y} \mathbf{X}^H = \mathbf{H} + \mathbf{N} \mathbf{X}^H, \quad (6)$$

which is similar to the SIMO model. Since  $\mathbf{X}$  is unitary, the noise distribution remains unaltered after this operation.

### A. 3GPP Channel Model

We consider different channel models in this work to validate the proposed methods. The 3rd Generation Partnership Project (3GPP) defines a spatial channel model for an urban macrocell scenario in which the transmit- and receive-side CCM is computed as [30]

$$\mathbf{C}_{\delta, \{\text{tx,rx}\}} = \int_{-\pi}^{\pi} g_{\{\text{tx,rx}\}}(\vartheta; \delta) \mathbf{a}_{\{\text{tx,rx}\}}(\vartheta) \mathbf{a}_{\{\text{tx,rx}\}}(\vartheta)^H d\vartheta. \quad (7)$$

The vector  $\mathbf{a}_{\{\text{tx,rx}\}}(\vartheta)$  denotes the array steering vector, which is  $[1, \exp(j\pi \sin(\vartheta)), \dots, \exp(j\pi(N_{\text{tx}}-1) \sin(\vartheta))]^H$  in the case of a ULA at the transmitter, and analogously at the receiver. The function  $g(\cdot; \delta)$  describes an angular power spectrum and is parameterized by the vector  $\delta$ , which follows a prior distribution  $p(\delta)$  that accounts for the involved path gains and angles of the propagation cluster. More precisely,  $g(\cdot; \delta)$  is a mixture of Laplace densities whose standard deviations represent the angular spreads. Each Laplace density represents a propagation cluster. The individual mean values and the weighting of the densities are formed by the corresponding angles and path gains, respectively. The angles are independent and identically distributed (i.i.d.) uniformly between  $-\pi/2$  and  $\pi/2$ . The path gains are as well i.i.d. uniformly between zero and one and are subsequently normalized such that they sum to one. The CCM for  $\mathbf{h}$  in (3) is obtained with (7) as  $\mathbf{C}_{\delta} = (\mathbf{C}_{\delta, \text{tx}} \otimes \mathbf{C}_{\delta, \text{rx}})$ , under the assumption of independent scattering in the vicinity of the transmitter and receiver [31]. In the case of the SIMO signal model,  $\mathbf{C}_{\delta}$  becomes  $\mathbf{C}_{\delta, \text{rx}}$ . Once the CCM is constructed, a CG channel can be obtained according to

$$\mathbf{h} | \delta \sim \mathcal{N}_{\mathbb{C}}(\mathbf{0}, \mathbf{C}_{\delta}). \quad (8)$$

This way, a dataset of CG channels is acquired to serve as training and validation data for the proposed methods. Note that  $\mathbf{C}_{\delta}$  is different for every channel, which causes the overall channel distribution  $p(\mathbf{h})$  to be non-Gaussian, although the channels themselves are CG.

### B. QuaDRiGa Channel Model

The QuaDRiGa channel simulator is developed by the Fraunhofer Heinrich-Hertz-Institute [32], [33]. It allows for the simulation of realistic channels in a randomized environment with spatial consistency and time evolution of channels. MIMO channel matrices are modeled as a superposition of  $L$  propagation paths such that

$$\mathbf{H} = \sum_{\ell=1}^L \mathbf{G}_{\ell} \exp(-2\pi j f_c \tau_{\ell}) \quad (9)$$

where the carrier frequency is denoted as  $f_c$  and the delay of the  $\ell$ -th path as  $\tau_{\ell}$ . The matrix  $\mathbf{G}_{\ell}$  expresses the complex-valued gain between every antenna pair and the antenna radiation pattern and polarization. After generation, the channels are post-processed to remove the path gain, as described in the QuaDRiGa documentation [33]. We use version 2.6.1 of

QuaDRiGa to simulate channels at a frequency of 6 GHz in an urban macrocell scenario. We place the BS at the height of 25 m, and it covers a sector of 120°. Twenty percent of the MTs are outdoors 1.5 m above the ground at a distance between 35 and 500 m from the BS. The remaining eighty percent are situated indoors at different floor levels. For line of sight (LOS), non-line of sight (NLOS), and outdoor-to-indoor propagation, the number of propagation paths in (9) is 37, 61, and 37, respectively. We equip the BS with “3GPP-3D” antennas and the MTs with omnidirectional antennas.

### C. Problem Formulation

In CE, the task is to estimate the channel  $\mathbf{h}$  based on the noisy pilot observation  $\mathbf{y}$  from (3). It is known that the CME

$$\hat{\mathbf{h}}_{\text{CME}}(\mathbf{y}) = \mathbb{E}[\mathbf{h} | \mathbf{y}] = \arg \min_{\hat{\mathbf{h}}} \mathbb{E} \left[ \|\mathbf{h} - \hat{\mathbf{h}}\|^2 \right] \quad (10)$$

results in MSE-optimal estimates [34, Ch. 11]. More generally, the CME is the optimal predictor for all Bregman loss functions, of which the MSE is a special case [35]. Application of Bayes rule to  $p(\mathbf{h} | \mathbf{y})$  yields

$$p(\mathbf{h} | \mathbf{y}) = \frac{p(\mathbf{y} | \mathbf{h}) p(\mathbf{h})}{p(\mathbf{y})} = \frac{p_{\mathbf{n}}(\mathbf{y} - \mathbf{A}\mathbf{h}) p(\mathbf{h})}{p(\mathbf{y})}, \quad (11)$$

which we use to rewrite (10) as

$$\mathbb{E}[\mathbf{h} | \mathbf{y}] = \int \mathbf{h} p(\mathbf{h} | \mathbf{y}) d\mathbf{h} = \int \mathbf{h} \frac{p_{\mathbf{n}}(\mathbf{y} - \mathbf{A}\mathbf{h}) p(\mathbf{h})}{p(\mathbf{y})} d\mathbf{h}. \quad (12)$$

Note that  $p_{\mathbf{n}}$  represents the distribution of  $\mathbf{n}$ . By inspection of (12), it becomes clear why the CME is difficult to compute. First, it requires access to the unknown and difficult-to-determine channel distribution  $p(\mathbf{h})$ , i.e.,  $p(\mathbf{h})$  must be estimated directly or indirectly. Second, an approximation of the integral in (12) is required since, in general, there exists no closed-form solution. This motivates the utilization of a VAE for CE since a VAE aims to learn  $p(\mathbf{h})$  and allows us to locally approximate the integral of the CME efficiently as will be shown in the next section.

## III. VAE-BASED CHANNEL ESTIMATION

### A. VAE Preliminaries

Variational inference (VI) builds the foundation of the VAE where the optimization of the evidence-lower bound (ELBO) is the central objective [36]. For this purpose, a parameterized likelihood model  $p_{\theta}(\mathbf{h})$  of the unknown distribution  $p(\mathbf{h})$  is typically decomposed as

$$\begin{aligned} \log p_{\theta}(\mathbf{h}) &= \mathbb{E}_{q_{\phi}(\mathbf{z} | \mathbf{y})} [\log p_{\theta}(\mathbf{h})] = \mathbb{E}_{q_{\phi}} \left[ \log \left( \frac{p_{\theta}(\mathbf{h}, \mathbf{z})}{p_{\theta}(\mathbf{z} | \mathbf{h})} \right) \right] \\ &= \mathbb{E}_{q_{\phi}} \left[ \log \left( \frac{p_{\theta}(\mathbf{h}, \mathbf{z})}{q_{\phi}(\mathbf{z} | \mathbf{y}) p_{\theta}(\mathbf{z} | \mathbf{h})} \right) \right] \\ &= \mathcal{L}_{\theta, \phi}(\mathbf{h}) + \text{D}_{\text{KL}}(q_{\phi}(\mathbf{z} | \mathbf{y}) \| p_{\theta}(\mathbf{z} | \mathbf{h})) \end{aligned} \quad (13)$$

with the ELBO

$$\mathcal{L}_{\theta, \phi}(\mathbf{h}) = \mathbb{E}_{q_{\phi}} [\log p_{\theta}(\mathbf{h}, \mathbf{z}) - \log q_{\phi}(\mathbf{z} | \mathbf{y})] \quad (14)$$

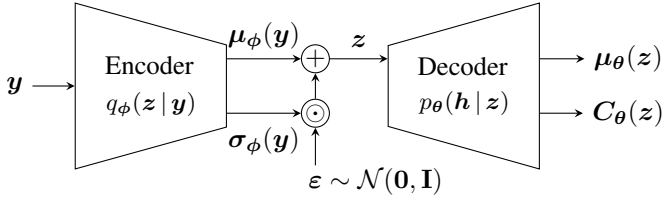


Fig. 1. Structure of a VAE with CG distributions for  $q_\phi(z|y)$  and  $p_\theta(h|z)$ . The encoder and decoder represent neural networks.

and the Kullback-Leibler (KL) divergence

$$D_{\text{KL}}(q_\phi(z|y) \| p_\theta(z|h)) = \mathbb{E}_{q_\phi} \left[ \log \left( \frac{q_\phi(z|y)}{p_\theta(z|h)} \right) \right]. \quad (15)$$

Note that  $\mathbb{E}_{q_\phi(z|y)}[\cdot] = \mathbb{E}_{q_\phi}[\cdot]$ . The subscripts  $\theta$  and  $\phi$  symbolize the parameterizations of the distributions. As an essential step, the VI framework introduces the variational distribution  $q_\phi(z|y)$ , which depends on the so-called hidden or latent vector  $z$ . The purpose of  $q_\phi(z|y)$  is to approximate the posterior distribution  $p_\theta(z|h)$  as closely as possible, which can be observed in (13) as a result of the KL term. Maximization of the ELBO achieves two goals: 1) the data log-likelihood is maximized, and 2) the KL divergence between  $q_\phi(z|y)$  and the posterior  $p_\theta(z|h)$  is minimized.

In contrast to conventional VI, the VAE optimizes the ELBO with the help of neural networks and the reparameterization trick [14], [15]. The VAE thus makes VI broadly accessible as it enables to process large amounts of data. The drawing in Fig. 1 illustrates the functionality of a VAE. For the training of a VAE, it is beneficial to express the ELBO as

$$\mathcal{L}_{\theta, \phi}(h) = \mathbb{E}_{q_\phi} [\log p_\theta(h|z)] - D_{\text{KL}}(q_\phi(z|y) \| p(z)). \quad (16)$$

The technical implementation of  $q_\phi(z|y)$  and  $p_\theta(h|z)$  is done by the corresponding encoder and decoder of the VAE, respectively, both realized by means of a neural network.

At this point, we must decide on the type and structure of the distributions that appear in (16). Common choices for them are CG distributions. Accordingly, the probability distributions involved are

$$\begin{aligned} p(z) &= \mathcal{N}(\mathbf{0}, \mathbf{I}), \\ p_\theta(h|z) &= \mathcal{N}_{\mathbb{C}}(\mu_\theta(z), C_\theta(z)), \\ \text{and } q_\phi(z|y) &= \mathcal{N}(\mu_\phi(y), \text{diag}(\sigma_\phi^2(y))). \end{aligned} \quad (17)$$

With these definitions, let us examine the underlying concept in more detail in Fig. 1. The encoder takes an observation  $y$  and maps it to the mean value  $\mu_\phi(y)$  and standard deviation vector  $\sigma_\phi(y)$  of  $q_\phi(z|y)$ . A sample  $\epsilon$  from a standard Gaussian distribution in combination with  $\mu_\phi(y)$  and  $\sigma_\phi(y)$  is used to obtain a reparameterized sample  $z = \mu_\phi(y) + \sigma_\phi(y) \odot \epsilon$ , the latent vector. The sample  $z \in \mathbb{R}^L$  is fed into the decoder to obtain the mean value  $\mu_\theta(z)$  and covariance matrix  $C_\theta(z)$  of the CG distribution  $p_\theta(h|z)$ . We denote the dimensionality of the latent space as  $L$ . Using the definitions in (17) allows us to find closed-form expressions for the terms in the ELBO. The expectation operation can be approximated with a single sample  $\tilde{z} \sim q_\phi(z|y)$ , i.e.,  $(-\mathbb{E}_{q_\phi} [\log p_\theta(h|z)])$  is replaced by the estimate

$$\log \det(\pi C_\theta(\tilde{z})) + (h - \mu_\theta(\tilde{z}))^\text{H} C_\theta^{-1}(\tilde{z})(h - \mu_\theta(\tilde{z})). \quad (18)$$

The KL-term  $D_{\text{KL}}(q_\phi(z|y) \| p(z))$  results in the closed form expression

$$\frac{1}{2} \left( \mathbf{1}^\text{T} (-\log \sigma_\phi^2(y) + \mu_\phi(y)^2 + \sigma_\phi^2(y)) - L \right). \quad (19)$$

It should be noted that the choice for the distribution  $p_\theta(h|z)$  in (17) differs from the standard implementation in the VAE literature. Almost all cases, the distribution is CG with a learnable mean vector and either a constant identity or a learnable diagonal covariance matrix. According to our definition (17), we intend to learn a full covariance matrix for the distribution  $p_\theta(h|z)$ . This way, the probabilistic modeling capability of the VAE is improved as we can model the correlations between the antennas, which would not be the case, e.g., for an identity or diagonal covariance matrix at the decoder. Depending on the system model, different parameterizations of  $C_\theta(z)$  should adequately approximate the true CCM. We will discuss this aspect in more detail in Section IV.

### B. MMSE Estimation with the VAE

After successfully training the VAE, we have a generative model that parameterizes the underlying channel distribution as CG. The key in this context is the condition. If we choose the condition adequately, we can make any random variable CG without restricting the expressivity of the model.<sup>1</sup> Finding a suitable condition can be challenging, particularly if the distribution of  $h$  is unknown. The VAE's goal is to assemble a CG channel via the latent vector  $z$  so that we have

$$h | z \sim p_\theta(h|z) = \mathcal{N}_{\mathbb{C}}(\mu_\theta(z), C_\theta(z)). \quad (20)$$

The CG relation in (20) resembles the CG relation from the 3GPP channel model in (8). However, this fundamental characteristic of the VAE-based channel estimator is neither motivated by the 3GPP channel model nor dependent on it in any way. On the contrary, the VAE learns an abstract condition  $z$  in its latent space that may not necessarily carry a physical interpretation, which implies that the VAE does not primarily target to approximate  $C_\delta$  with  $C_\theta(z)$ . The advantage of the abstractness of the condition is the flexibility to model the channels as CG since the model can select an almost arbitrary condition for every channel. The VAE approximates the channel distribution this way. Indeed, the CG property will be beneficial for the design of the proposed channel estimator.

Section II-C points out that the CME provides MMSE channel estimates. Applying the law of total expectation, these estimates can be reformulated as

$$E[h|y] \approx \int p_\theta(z|y) E[h|z, y] dz = E_z [E[h|z, y] | y], \quad (21)$$

where we replaced  $p(z|y)$  with its parameterized approximation  $p_\theta(z|y)$ . Then, assuming the trained VAE achieves its goal and (20) holds, we obtain a closed-form expression

<sup>1</sup>CG might seem like a limitation at first thought. We elaborate on this relation with the following toy example. To this end, consider the random variable  $h$  from an unknown distribution and its observation  $h - t$ . Knowing that  $t$  is a Gaussian random variable,  $h | (h - t)$  becomes CG.

for the inner expectation due to the CG property. Therefore,  $E[\mathbf{h} | \mathbf{z}, \mathbf{y}]$  results in [34, Ch. 11]:

$$\boldsymbol{\mu}_{\theta}(\mathbf{z}) + \mathbf{C}_{\theta}(\mathbf{z}) \mathbf{A}^H (\mathbf{A} \boldsymbol{\mu}_{\theta}(\mathbf{z}) + \boldsymbol{\Sigma})^{-1} (\mathbf{y} - \mathbf{A} \boldsymbol{\mu}_{\theta}(\mathbf{z})), \quad (22)$$

where the matrix  $\mathbf{A}$  and vector  $\mathbf{y}$  belong to the system model in (3). Note that  $\mathbf{z}$  depends on  $\mathbf{y}$  through the encoder and  $\boldsymbol{\mu}_{\theta}(\mathbf{z})$  and  $\mathbf{C}_{\theta}(\mathbf{z})$  are provided by the decoder of the VAE. Since the inner expectation can be computed in closed-form via (22), it remains to solve the outer expectation, i.e., the integral in (21). To calculate the integral access to  $p_{\theta}(\mathbf{z} | \mathbf{y})$  is required. The latter is approximated by  $q_{\phi}(\mathbf{z} | \mathbf{y})$ , which finds its justification in (15) via the KL divergence to  $p_{\theta}(\mathbf{z} | \mathbf{h})$  that vanishes with increasing VAE learning. Although the evaluation of (21) based on  $q_{\phi}(\mathbf{z} | \mathbf{y})$  introduces another approximation uncertainty, the excellent estimation results observed in Section VI justify this measure. Thus, replacing  $p_{\theta}(\mathbf{z} | \mathbf{y})$  by  $q_{\phi}(\mathbf{z} | \mathbf{y})$  in (21), we obtain

$$E[\mathbf{h} | \mathbf{y}] \approx E_{q_{\phi}}[t_{\theta}(\mathbf{z}, \mathbf{y})], \quad t_{\theta}(\mathbf{z}, \mathbf{y}) = E[\mathbf{h} | \mathbf{z}, \mathbf{y}] \quad (23)$$

and assume that the KL divergence in (15) is minimized. As we can easily obtain samples of  $q_{\phi}(\mathbf{z} | \mathbf{y})$  with the help of the encoder, we can approximate  $E[\mathbf{h} | \mathbf{y}]$  using samples of the form  $\mathbf{z}^{(k)} = \boldsymbol{\mu}_{\theta}(\mathbf{y}) + \boldsymbol{\varepsilon}^{(k)} \odot \boldsymbol{\sigma}_{\theta}(\mathbf{y})$  where every  $\boldsymbol{\varepsilon}^{(k)}$  is a sample from  $\mathcal{N}(\mathbf{0}, \mathbf{I})$ ,  $k = 1, \dots, K$ . Based on the samples  $\mathbf{z}^{(k)}$  we can asymptotically approximate the MMSE channel estimator as a consequence of the law of large numbers [37]:

$$\hat{h}_{\text{VAE}}^{(K)}(\mathbf{y}) = \frac{1}{K} \sum_{k=1}^K t_{\theta}(\mathbf{z}^{(k)}, \mathbf{y}), \quad \mathbf{z}^{(k)} \sim q_{\phi}(\mathbf{z} | \mathbf{y}), \quad (24)$$

where  $t_{\theta}(\mathbf{z}^{(k)}, \mathbf{y})$  is evaluated with (22)

The estimate  $\hat{h}_{\text{VAE}}^{(K)}(\mathbf{y})$  generally becomes better for a large number of samples  $K$ , which is unwanted in a real-time system. It is desirable to reduce the complexity of the estimator as much as possible, which means that  $K$  should be low. We show that a single sample already yields adequate estimation performance by investigating different  $K$  in Section VI-A. A single sample implies  $K = 1$  and is the least complex way to obtain the sample-based estimate. If we have to choose exactly one sample from  $q_{\phi}(\mathbf{z} | \mathbf{y})$  for the evaluation of  $\hat{h}_{\text{VAE}}^{(K)}(\mathbf{y})$ , the obvious choice is the mean vector  $\boldsymbol{\mu}_{\phi}(\mathbf{y})$ . In our simulations, we observe that the variance  $\boldsymbol{\sigma}_{\phi}^2(\mathbf{y})$  of  $q_{\phi}(\mathbf{z} | \mathbf{y})$  is small after training the VAE. Consequently, the sampling process in (24) mostly returns samples close to  $\boldsymbol{\mu}_{\phi}(\mathbf{y})$ . This justifies the usage of a single sample  $\mathbf{z}^{(1)} = \boldsymbol{\mu}_{\phi}(\mathbf{y})$  and results in the approximation

$$\hat{h}_{\text{VAE}}(\mathbf{y}) = \hat{h}_{\text{VAE}}^{(1)}(\mathbf{y}) = t_{\theta}(\mathbf{z}^{(1)}) = \boldsymbol{\mu}_{\phi}(\mathbf{y}), \quad (25)$$

of the MMSE estimator. Unless otherwise stated, we use the estimator in (25) for the numerical simulations in this work.

Given the estimation results in Section VI based on (25), a brief description and interpretation of how and why the estimator works excellently follows. Although using the mean  $\boldsymbol{\mu}_{\phi}(\mathbf{y})$  seems obvious when considering only a single Monte Carlo sample, this does not yet explain its strong performance. The necessary reformulation that must be applied to the estimator in (23) to yield (25) reads as

$$E_{q_{\phi}}[t_{\theta}(\mathbf{z}, \mathbf{y})] = t_{\theta}(E_{q_{\phi}}[\mathbf{z}], \mathbf{y}), \quad (26)$$

with

$$t_{\theta}(E_{q_{\phi}}[\mathbf{z}], \mathbf{y}) = t_{\theta}(\boldsymbol{\mu}_{\phi}(\mathbf{y}), \mathbf{y}). \quad (27)$$

Note that the relation in (26) is Jensen's inequality for the special case where equality holds, which is the case if and only if  $t_{\theta}(\mathbf{z}, \mathbf{y})$  is linear in  $\mathbf{z}$  on a convex set. In other words, the estimator  $\hat{h}_{\text{VAE}}(\mathbf{y})$  assumes that (23) is linear in  $\mathbf{z}$  in the neighborhood of  $\boldsymbol{\mu}_{\phi}(\mathbf{y})$ . Since the latent space of the VAE is continuous and thus, for every input sample, there is a different latent encoding, the assumption of linearity around the latent mean of one sample is not contradictory to the overall expressiveness of the VAE. Our results do not prove that linearity in  $\mathbf{z}$  around  $\boldsymbol{\mu}_{\phi}(\mathbf{y})$  can be identified for  $t_{\theta}(\mathbf{z}, \mathbf{y})$ . The elaborations in this paragraph are, however, a supporting argument for this conjecture and a justification why  $\hat{h}_{\text{VAE}}(\mathbf{y})$  can deliver strong CE results based on the single sample  $\boldsymbol{\mu}_{\phi}(\mathbf{y})$  from  $q_{\phi}(\mathbf{z} | \mathbf{y})$ .

### C. MSE-Optimality

Inspired by the universal approximation properties of neural networks, see, e.g., [38], [39], and the analysis of the asymptotic optimality of the GMM-based channel estimator in [18], the convergence behavior of the VAE-based channel estimator to the MSE-optimal CME is studied in this section. First, we state a helpful definition of the universal approximation theorem in terms of the uniform convergence of functions based on the results from [38], [39], which consider networks of arbitrary depth and bounded width. Note that we do not discuss the exact bounds on the width of the networks since it is no primary subject of our discussion.

**Definition 1** (Universal Approximation). *Let  $\mathcal{C}(\mathbb{X}, \mathbb{Y})$  denote the set of continuous functions from  $\mathbb{X}$  to  $\mathbb{Y}$ , and  $\xi : \mathbb{R} \rightarrow \mathbb{R}$  be any non-affine continuous activation function (e.g., ReLU). Let  $\mathcal{F}_{\ell}$  denote the space of feed-forward neural networks with  $d_{\text{in}}$  input and  $d_{\text{out}}$  output neurons with  $\ell$  layers, each with a predetermined, finite number of neurons, where every hidden layer has the activation function  $\xi$  and the output has an identity activation function. Then, for any  $f \in \mathcal{C}(\mathcal{X}, \mathbb{R}^{d_{\text{out}}})$ , where  $\mathcal{X}$  is a compact subset of  $\mathbb{R}^{d_{\text{in}}}$ , there exists a sequence  $(f^{(\ell)})_{\ell=2}^{\infty}$  with  $f^{(\ell)} \in \mathcal{F}_{\ell}$  such that*

$$\lim_{\ell \rightarrow \infty} \|f^{(\ell)} - f\|_{\infty} = 0. \quad (28)$$

Consequently, by invoking the universal approximation ability from Definition 1, one may assume the existence of sequences of functions that parameterize the distributions of the encoder and decoder of the VAE. More precisely, we consider  $q_{\phi}^{(\eta)}(\mathbf{z} | \mathbf{h})$  and  $p_{\theta}^{(\tau)}(\mathbf{h} | \mathbf{z})$ , where  $\eta$  and  $\tau$  are the numbers of layers of the encoder and decoder DNNs, respectively, such that they converge uniformly to the true underlying distribution functions according to

$$\lim_{\eta \rightarrow \infty} \|q_{\phi}^{(\eta)}(\mathbf{z} | \mathbf{h}) - p(\mathbf{z} | \mathbf{h})\|_{\infty} = 0, \quad (29)$$

$$\lim_{\tau \rightarrow \infty} \|p_{\theta}^{(\tau)}(\mathbf{h} | \mathbf{z}) - p(\mathbf{h} | \mathbf{z})\|_{\infty} = 0. \quad (30)$$

The distribution  $q_{\phi}^{(\eta)}$  is conditioned on  $\mathbf{h}$  here, instead on  $\mathbf{y}$ , to stress its approximation to  $p(\mathbf{z} | \mathbf{h})$ , which relates to the

VAE-genie variant introduced in Section IV-A. Furthermore, these functions parameterize a distribution

$$p_{\phi, \theta}^{(\eta, \tau)}(\mathbf{h}) = \frac{p_{\theta}^{(\tau)}(\mathbf{h} | \mathbf{z}) p(\mathbf{z})}{q_{\phi}^{(\eta)}(\mathbf{z} | \mathbf{h})} \quad (31)$$

which approximates the underlying data distribution  $p(\mathbf{h})$  as shown in the following.

**Theorem 1.** *Let  $\mathbf{h} \in \mathcal{X}$  where  $\mathcal{X}$  is a compact subset of  $\mathbb{R}^N$ , let  $p(\mathbf{h}) \in \mathcal{C}(\mathcal{X}, \mathbb{R})$  be arbitrary, and let (29) and (30) hold. Then, the universal approximation properties of the distributions  $q_{\phi}^{(\eta)}$  and  $p_{\theta}^{(\tau)}$  imply the uniform convergence of the parameterized data distribution  $p_{\phi, \theta}^{(\eta, \tau)}$  from (31) to the true data distribution in the sense that*

$$\lim_{\eta, \tau \rightarrow \infty} \|p_{\phi, \theta}^{(\eta, \tau)}(\mathbf{h}) - p(\mathbf{h})\|_{\infty} = 0. \quad (32)$$

*Proof:* See Appendix A.

In [18, Th. 2], it is shown that the CME approximation via an estimator based on a GMM which is learned on the underlying channel distribution, converges uniformly to the true CME when the number of mixture components goes to infinity. The key prerequisite for this result is the uniform convergence of the GMM-approximated distribution to the true channel distribution due to the universal approximation properties of GMMs. Building on the result from Theorem 1 together with [18, Th. 2], we can state the asymptotic optimality of the VAE-based channel estimator in the following Corollary.

**Corollary 1.** *Let  $p(\mathbf{h}) \in \mathcal{C}(\mathcal{X}, \mathbb{R})$  be arbitrary as defined before and let  $\mathbf{A} \in \mathbb{R}^{N \times N}$  be invertible. Then, the VAE-parameterized CME approximation, defined as*

$$\hat{\mathbf{h}}_{\text{VAE}}^{(\tau, \eta)}(\mathbf{y}) = \mathbb{E}^{(\tau, \eta)}[\mathbf{h} | \mathbf{y}] = \int \mathbf{h} \frac{p_{\mathbf{n}}(\mathbf{y} - \mathbf{A}\mathbf{h}) p_{\phi, \theta}^{(\eta, \tau)}(\mathbf{h})}{p_{\phi, \theta}^{(\eta, \tau)}(\mathbf{y})} d\mathbf{h}, \quad (33)$$

approximates the CME from (21) in the sense that

$$\lim_{\eta, \tau \rightarrow \infty} \|\hat{\mathbf{h}}_{\text{VAE}}^{(\tau, \eta)}(\mathbf{y}) - \hat{\mathbf{h}}_{\text{CME}}(\mathbf{y})\| = 0 \quad (34)$$

holds for any given  $\mathbf{y} \in \mathbb{R}^N$ .

*Proof.* The proof is a direct consequence of [18, Th. 2] together with the uniform convergence from Theorem 1.  $\square$

*Discussion:* The result of Corollary 1 is, first of all, an indicator of the powerful capabilities and the potential of the VAE-based channel estimator. However, it does not directly quantify the possible performance in the non-asymptotic case in a practical application. A critical aspect thereby is that the approximations of the distributions in (29) and (30) are not explicitly targeted by the cost function in the training of the VAE. Furthermore, the practical evaluation of the estimator, due to the continuous nature of the latent space, always remains an approximation of the true CME. In this context, it is worth noting that the convergence analysis in this section may as well be carried out for a DNN that tries to learn the posterior  $p(\mathbf{h} | \mathbf{y})$  to approximate the CME from (10) by means of a regression network. That said, the results of Theorem 1 and Corollary 1 prove that the VAE framework does not

diminish the theoretical capabilities of converging to the CME concerning such a regression approach. Moreover, the VAE directly learns an approximation to the unconditioned channel distribution, arguably resulting in better generalization abilities and convergence properties. The excellent simulation results in Section VI support this argumentation, where we show the performance of the non-asymptotic implementation that verifies the discussion.

#### IV. PRACTICAL ASPECTS

In principle, we train a VAE with the loss in (16), and, after the training, perform CE as described in the previous section. Certain hurdles exist in the practical evaluation, which we want to address in this section.

During the training and estimation, the matrix  $\mathbf{C}_{\theta}(\mathbf{z})$  must be inverted, either directly as in (18) or a transformed version of it as in (22). Therefore, it is preferable to simplify the inversion process. To this end, we consider circulant matrices in this paper, which are unitary and whose inverses are easy to determine [29]. Circulant matrices are asymptotic approximators of Toeplitz matrices of large dimensions. Toeplitz matrices, in turn, are justified by the assumption of a ULA in the underlying application at both the BS and MT. Due to the uniform spacing, the CCM of a ULA is Toeplitz structured. In the MIMO signal model, we model the CCM as a Kronecker product of a transmit- and receive-side circulant CCM under the assumption of independent scattering in the vicinity of the BS and MT, cf. [31]. The Kronecker assumption motivates us to model the CCM of  $p_{\theta}(\mathbf{h} | \mathbf{z})$  as a block-circulant matrix in the realization of the VAE in Fig. 1. More precisely, we model the CCM as

$$\mathbf{C}_{\theta}(\mathbf{z}) = \mathbf{Q}^H \text{diag}(\mathbf{c}_{\theta}(\mathbf{z})) \mathbf{Q}, \quad \mathbf{c}_{\theta}(\mathbf{z}) \in \mathbb{R}_+^N \quad (35)$$

where  $\mathbf{Q} = (\mathbf{F}_{N_{\text{tx}}} \otimes \mathbf{F}_{N_{\text{rx}}})$  and  $\mathbf{F}_m \in \mathbb{C}^{m \times m}$  is a DFT matrix. The matrix  $\mathbf{Q}$  is again unitary as it is a Kronecker product of two unitary matrices. The parameterization in (35) requires only the determination of an  $N$ -dimensional positive real-valued vector to obtain a complete covariance matrix. In this case, the decoder outputs  $\mathbf{c}_{\theta}(\mathbf{z})$ . Finally, the block-circulant parameterization in (35) simplifies to a conventional circulant parameterization

$$\mathbf{C}_{\theta}(\mathbf{z}) = \mathbf{F}_{N_{\text{rx}}}^H \text{diag}(\mathbf{c}_{\theta}(\mathbf{z})) \mathbf{F}_{N_{\text{rx}}}, \quad \mathbf{c}_{\theta}(\mathbf{z}) \in \mathbb{R}_+^{N_{\text{rx}}} \quad (36)$$

in the SIMO signal model case, since the matrix  $\mathbf{Q}$  then becomes an ordinary DFT matrix  $\mathbf{F}_{N_{\text{rx}}}$ .

For the training of DL models, it is beneficial to provide sparse inputs. To this end, the observation matrix  $\mathbf{Y}$  is first multiplied with the inverse of the pilot matrix  $\mathbf{X}^H$  from the right as in (6). The relation in (6) is afterward vectorized and multiplied with  $\mathbf{Q}$  from the left, which performs a 2D DFT, and reshaped as a matrix, reversing the vectorization. Similarly, the negative decoder log-likelihood in (18) can be further simplified by using  $\mathbf{h}_Q = \mathbf{Q}\mathbf{h}$ , which yields

$$N \log \pi + \mathbf{1}^T (\boldsymbol{\lambda}_{\theta}(\mathbf{z}) \odot |\mathbf{h}_Q - \mathbf{Q}\boldsymbol{\mu}_{\theta}(\mathbf{z})|^2 - \log \boldsymbol{\lambda}_{\theta}(\mathbf{z})). \quad (37)$$

with  $\boldsymbol{\lambda}_{\theta}(\mathbf{z}) = \mathbf{c}_{\theta}^{-1}(\mathbf{z})$  and the element-wise absolute value  $|\cdot|$ . The expression in (37) significantly reduces the numerical

complexity of the training process because it avoids the repeated inversion of a full covariance matrix.

A common assumption we also make here is white noise, which yields  $\Sigma = \varsigma^2 \mathbf{I}$ , with the noise variance  $\varsigma^2$  assumed to be given in our experiments.

### A. Variants of VAE-based Channel Estimators

We present three possible channel estimators in the following that leverage the VAE. All three estimators have in common that the VAEs can be trained offline before applying them to CE. The estimators differ in their knowledge of the channel state information (CSI) during the training and evaluation phase.

1) *VAE-genie*: To determine the full potential of our method, we assume  $\mathbf{n} = \mathbf{0}$  for the input  $\mathbf{y}$  of the encoder, which becomes  $\mathbf{h}$  after decorrelating the pilots and vectorizing. This changes the variational distribution to  $q_\phi(\mathbf{z} | \mathbf{h})$ . Hence, VAE-genie directly relates to the MSE-optimality analysis from Section III-C. VAE-genie is supposed to exhibit the best estimation results among all variants because the conditional mean vector and covariance matrix at the decoder are inferred with the actual channel at the encoder and its latent representation. Hence, the latent representation is most informative about the channel in this case. Although VAE-genie even has the potential to outperform the CME, as perfect CSI acts as side information, this estimator is not applicable to a real scenario since it requires CSI knowledge during the evaluation phase. Instead, it inspires the basic idea of the proposed method. It can serve as a suitable benchmark result in a CE scenario where the optimal estimator is unknown and inaccessible. VAE-genie requires CSI knowledge during the training *and* evaluation phase.

2) *VAE-noisy*: This version of the VAE channel estimator is precisely the one pictured in Fig. 1. The encoder receives  $\mathbf{y}$  as input. VAE-noisy only requires CSI knowledge during the training phase to compute  $p_\theta(\mathbf{h} | \mathbf{z})$ . During the evaluation phase, the mean value  $\mu_\phi(\mathbf{y})$  is obtained based on the noisy observation to compute (22), which is the reason for the name of this estimator. We expect that VAE-noisy delivers worse estimation quality than VAE-genie as VAE-genie has access to the true channel in the evaluation phase. VAE-noisy is, in contrast, applicable in practice.

3) *VAE-real*: Similar to VAE-noisy, this variant of the estimator also receives  $\mathbf{y}$  as input at the encoder. The change compared to VAE-noisy happens at the decoder where VAE-real learns a mean value and covariance matrix for  $p_\theta(\mathbf{y} | \mathbf{z})$  instead of  $p_\theta(\mathbf{h} | \mathbf{z})$ . Consequently, VAE-real maximizes a lower bound to  $p_\theta(\mathbf{y})$ . However, to efficiently compute  $E[\mathbf{h} | \mathbf{z}, \mathbf{y}]$  we need a CG model for  $\mathbf{h}$  and not  $\mathbf{y}$ . Regarding  $\mu_\theta(\mathbf{z})$  in (22), this is not a problem as long as  $E[\mathbf{n}] = \mathbf{0}$ , which is the case in (3). A simple workaround can determine the conditional CCM. While the VAE decoder continues to output  $\mathbf{c}_\theta(\mathbf{z})$ , the covariance matrix  $\mathbf{Q}^H(\text{diag}(\mathbf{c}_\theta(\mathbf{z})) + \varsigma^2)\mathbf{Q}$  is used instead to compute  $p_\theta(\mathbf{y} | \mathbf{z})$  during training. The vector  $\varsigma^2$  is a vector where all elements are equal to  $\varsigma^2$ . This way, the decoder's learning algorithm forces to substitute only the desired part, the conditional CCM  $\mathbf{C}_\theta(\mathbf{z})$ . We enforce

TABLE I  
HYPERPARAMETERS FOR THE NEURAL NETWORKS THAT CONSTITUTE THE ENCODER AND DECODER OF THE VAE.

	$N_{\text{rx}} = 128$ (SIMO)	$N_{\text{rx}} = 32, N_{\text{tx}} = 4$
channels input	48	48
channel mult.	1.75	1.75
kernel size	9	[5, 2]
padding	1	2
batch size	128	128
latent dimension	16; 32	16; 32
learning rate	7e-4	7e-4
stride	2	2
activation func.	ReLU	ReLU

that the decoder outputs the conditional CCM by training solely on noisy observations  $\mathbf{y}$  at the encoder and decoder. It should be noted that no access to the noise-free, ground-truth channels is needed by VAE-real, neither during training nor during evaluation. VAE-real is the most realistic estimator since pilot observations from the regular operation of the BS can be utilized to train the VAE. In contrast, having access to noise-free CSI during the training phase requires either costly measurement campaigns or artificially generated data with an unavoidable mismatch to real-world data.

Combining every aspect from this and the previous section, the objective function that VAE-genie and VAE-noisy are supposed to minimize during the training is:

$$\mathcal{L}_{\theta, \phi} = \mathbf{1}^T [\lambda_\theta(\mathbf{z}) \odot |\mathbf{h}_Q - \mathbf{Q}\mu_\theta(\mathbf{z})|^2 - \log \lambda_\theta(\mathbf{z}) - \log \sigma_\phi(\mathbf{y}) + 0.5(\mu_\phi(\mathbf{y})^2 + \sigma_\phi^2(\mathbf{y}))]. \quad (38)$$

We omit the argument and constants for brevity. For the training of VAE-real, in (38),  $\mathbf{h}_Q$  is replaced with  $\mathbf{y}_Q = \mathbf{Q}\mathbf{A}^H \mathbf{y}$ , and  $\lambda_\theta(\mathbf{z})$  with  $(\mathbf{c}_\theta(\mathbf{z}) + \varsigma^2)^{-1}$ . None of the proposed estimators tries to learn a direct regression mapping from a noisy pilot observation to a channel estimate. The proposed methods aim to learn the channel distribution and exploit the CG property of the VAE to parameterize an estimator.

### B. VAE Architecture

We briefly describe our VAE implementation in this section. The simulation code with the corresponding architectures is also publicly available<sup>2</sup>. Fig. 2 illustrates the VAE implementation. Table I outlines hyperparameters, to which we refer in this section, and are integrated into the architecture. For brevity, we only show the hyperparameters for the most relevant system configurations, i.e., the SIMO model with 128 antennas at the receiver and the MIMO model with 32 and 4 antennas at the receiver and transmitter, respectively. Any other architecture is accessible in the online repository. The colorings of the arrows in Fig. 2 symbolize different standard layers. On the left, it is visible that the real and imaginary parts of the encoder input are stacked as convolutional channels (CCs). As a first block, the purple arrow  represents a 1x1 convolutional layer (CL) that maps to a higher number of CCs, which is the number in the first row of Table I,

<sup>2</sup><https://github.com/tum-msv/vae-estimator>.

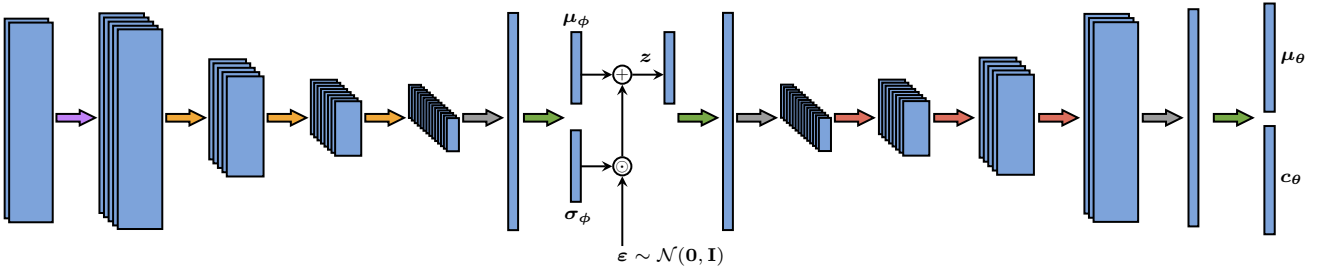


Fig. 2. Detailed illustration of the different layers constituting our VAE implementation. The real and imaginary parts of the input are stacked as CCs and processed. Each colored arrow represents a different standard layer. Purple  $\Rightarrow$  stands for a  $1 \times 1$  CL, orange  $\Rightarrow$  for a block of a CL, BN layer, and ReLU activation function, gray  $\Rightarrow$  for a RL, green  $\Rightarrow$  for a LL, and red  $\Rightarrow$  for a block of a transposed CL, BN layer, and ReLU activation function.

labeled ‘channels input.’ Subsequently, three orange arrows  $\Rightarrow$  follow, representing a block of a CL, a batch normalization (BN) layer, and a ReLU activation function. In the CL, the CC amount at the output is multiplied by a factor of 1.75, which is in the second row of Table I, compared to the amount at the input. After a reshaping layer (RL) and linear layer (LL), symbolized by the gray arrow  $\Rightarrow$  and green arrow  $\Rightarrow$ , respectively, we arrive at the latent space. The reparameterized sample  $z$  is fed into the decoder, which is a symmetrically flipped version of the encoder. That means  $z$  is first brought into the same shape as before the last gray arrow  $\Rightarrow$  to the left with an LL and RL. Second, three blocks of a transposed CL, a BN layer, and a ReLU activation function, symbolized by the red arrows  $\Rightarrow$ , process the sample. The amount of CCs is reduced by the same factor of 1.75 after each block. In the end, we have a sample with three CCs that is fed into a RL and LL to produce the outputs of the decoder.

If not otherwise stated, Table I depicts the kernel size in all CLs. The kernel sizes highlight that we use 2D CLs in the MIMO case and 1D CLs in the SIMO case. A batch size of 128, a learning rate of 7e-4 in combination with Adam [40], and a stride of 2 in the CLs is used. The dimension of the latent space is 16 for settings with one dominant propagation path and 32 for the remaining cases. The values in Table I were found by a random search over the hyperparameter space by searching for the combination that yields the highest value for (37) [41]. We perform the random search with the help of the *Tune* package [42]. Interestingly, a large value for (37) coincides with strong estimation results. We implement the DNNs with PyTorch. Additionally, we experimented with BN and its variants to determine how we can achieve the best performance [43]–[45]. We achieve the best performance with BN as is proposed in [43]. The only important point is to consider a large enough batch size to limit the variance of the stochastic gradient, which is the case for the batch size in Table I. We additionally use the method of free bits during the training as described in [40].

### C. Computational Complexity

In this section, we discuss the computational complexity of the proposed estimator. The procedure to determine  $\hat{h}_{\text{VAE}}$  can be split into two parts. The first step is a forward pass through the VAE to acquire  $\mu_{\theta}(z)$  and  $C_{\theta}(z)$ . The second step is the evaluation of  $t_{\theta}(z, y)$  in (22) with given  $\mu_{\theta}(z)$

and  $C_{\theta}(z)$ . The computational complexity of the first step is tied to the VAE architecture in Fig. 2. Since all layers exhibit a different complexity, we need a complexity bound for which three computations are relevant. The first relevant operation is the decorrelation of the pilots in (6), which has a complexity of  $\mathcal{O}(N_{\text{tx}} \log N_{\text{tx}})$ . A multiplication with  $Q$  in  $\mathcal{O}(N \log N)$  time follows as it is identical to a DFT with  $N$  coefficients. A CL requires  $\mathcal{O}(RN)$  time, with  $R$  being the product of the number of parameters divided by the stride in the CL. The final LL requires  $\mathcal{O}(N^2)$  time. The remaining layers exhibit less complexity than the CLs and final LL. Although  $R$  should be increased if  $N$  grows,  $R$  does not show more than linear growth in  $N$ . In conclusion, utilizing  $\mathcal{O}(N^2)$  as complexity bound per layer is reasonable. For the  $D$  layers of the VAE forward pass, this makes an overall complexity of  $\mathcal{O}(DN^2)$ .

We come to the second step of obtaining  $\hat{h}_{\text{VAE}}$ , which is the evaluation of  $t_{\theta}(z, y)$ . In principle, the inversion of  $AC_{\theta}(z)A^H + \varsigma^2 I$  dominates the complexity. Let us inspect

$$AC_{\theta}(z)A^H = (X^T \otimes I_{N_{\text{tx}}})Q^H \text{diag}(c_{\theta}(z))Q(X^* \otimes I_{N_{\text{tx}}}) \quad (39)$$

in more detail. If we assume to have a DFT matrix as pilots, i.e.,  $X = F_P$ , and set  $\tilde{A} = AQ^H = (X^T \otimes I_{N_{\text{tx}}})Q^H$  we can show that  $\tilde{A}\tilde{A}^H = I$  and  $\tilde{A}^H\tilde{A} = I$  holds, so  $\tilde{A}$  is unitary. Hence, the inverse of  $AC_{\theta}(z)A^H$  is  $\tilde{A} \text{diag}(c_{\theta}^{-1}(z))\tilde{A}^H$ . We can therefore simplify the estimate  $t_{\theta}(z, y)$  as in (22) to

$$\mu_{\theta}(z) + Q^H \text{diag}(I + c_{\theta}(z) \odot \varsigma^{-2})Q(A^H y - \mu_{\theta}(z)) \quad (40)$$

whose complexity boils down to matrix-vector multiplications. It remains to clarify the complexity of multiplication with  $Q$  as  $A^H y$  is the pilot decorrelation we already performed in the forward pass of the VAE. The complexity of multiplication with  $Q$  is again  $\mathcal{O}(N \log N)$ .

As can be seen from our elaborations above, the evaluation of the VAE requires  $\mathcal{O}(DN^2)$  time, which outweighs the evaluation time of  $\mathcal{O}(N \log N)$  for (40). In this work, we did not optimize the VAE architectures for low complexity estimation but for best estimation performance. Many potentials exist to reduce the VAE complexity, e.g., with pruning [46]. Moreover, the computations in the VAE are highly parallelizable due to the CLs, which mitigates the  $\mathcal{O}(DN^2)$  complexity.

## V. RELATED CHANNEL ESTIMATORS

This section presents both classical and ML-based channel estimators for comparison. In the case of the 3GPP channel

model from Section II-A, we have access to the CCM  $\mathbf{C}_\delta$  from which the CG channel is sampled in (8). This allows us to evaluate the conditional mean estimator [7], which is given by the LMMSE formula

$$\hat{\mathbf{h}}_{\text{genie-cov}} = \mathbf{C}_\delta \mathbf{A}^H (\mathbf{A} \mathbf{C}_\delta \mathbf{A}^H + \Sigma)^{-1} \mathbf{y}, \quad (41)$$

and represents the MMSE estimator for the CG channel. We name this estimator *genie-cov* as it uses utopian genie knowledge to acquire the true CCM.

A practical estimator can be based on the sample covariance matrix  $\hat{\mathbf{C}} = \frac{1}{T_r} \sum_{i=1}^{T_r} \mathbf{h}_i \mathbf{h}_i^H$  for  $T_r$  samples in the training dataset. The corresponding estimator reads as

$$\hat{\mathbf{h}}_{\text{global-cov}} = \hat{\mathbf{C}} \mathbf{A}^H (\hat{\mathbf{C}} \mathbf{A}^H + \Sigma)^{-1} \mathbf{y}. \quad (42)$$

It is interesting to see the performance of the proposed estimator compared to the genie-cov estimator because the proposed estimator learns individual CCMs, similar to (41). The other extreme marks the global-cov estimator, where every estimation task shares the same learned CCM.

Least squares (LS) estimation is another comparison method we investigate in our simulations. A LS estimate can be obtained as  $\hat{\mathbf{h}}_{\text{LS}} = \mathbf{A}^+ \mathbf{y}$  with the pseudoinverse  $\mathbf{A}^+$ .

Compressed sensing (CS)-based CE techniques are another prominent topic in the literature. Especially regarding millimeter waves, CS algorithms are potentially interesting candidates [47]. In this work, we compare the proposed estimators with the approximate message passing (AMP) algorithm [48], [49]. One benefit of AMP is that the algorithm automatically finds the sparsity level. As a dictionary for AMP, we use a two times oversampled DFT matrix. AMP is a popular method in the CE literature in combination with CS.

We also want to compare the proposed estimators with current ML-based channel estimators. A recently proposed method exploits structural information of the MMSE estimator to design a neural network-based estimator for the SIMO signal model [7]. The derivation leads to a convolutional neural network with ReLU activation function, so we call this estimator CNN. The extension of [7] to the MIMO case is proposed in [50], to which we also refer in our simulations.

The last comparison method in this section, also recently proposed, is based on a GMM [18]. The idea is to fit a GMM to the underlying channel distribution and parameterize a channel estimator with the help of the GMM. The method is related to our estimator as its basis also is to learn the channel distribution. However, the methods are also very different because the GMM utilizes a discrete latent space and the VAE a continuous latent space. The parameterization of the estimator also differs substantially. It is still interesting to see the methods compete with each other as they both parameterize approximations to the CME. The GMM estimator is extended to fit its GMM parameters solely based on noisy pilot observations in [28], similar to the proposed VAE-real variant. Our evaluations in the next section will demonstrate that the VAE-real variant exhibits almost identical performance as the VAE-noisy variant, which has access to ground-truth channel data during the training. Therefore, we only evaluate the GMM estimator in [18]. We fit a GMM with 128 mixture components for all simulations.

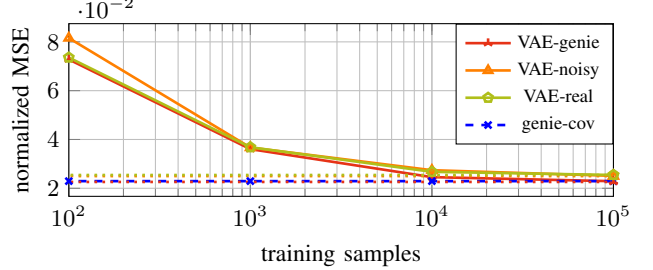


Fig. 3. Normalized MSE for different numbers of training samples at an SNR of 10dB for the 3GPP SIMO channel model with three propagation clusters and 128 antennas at the receiver. The dotted lines display the achieved result with the complete training dataset of 180,000 samples.

## VI. SIMULATION RESULTS

This section presents the CE results based on numerical simulations. We create 200,000 channel realizations for every system configuration in the upcoming section. The channels are divided into  $T_r = 180,000$  training,  $T_v = 10,000$  validation, and  $T_e = 10,000$  test samples. The channels are normalized such that  $E[\|\mathbf{h}\|^2] = N$ . In all our experiments, we calculate the normalized mean squared error (NMSE) as

$$\text{NMSE} = \frac{E[\|\mathbf{h} - \hat{\mathbf{h}}\|^2]}{E[\|\mathbf{h}\|^2]} = \frac{1}{T_e N} \sum_{i=1}^{T_e} \|\mathbf{h}_i - \hat{\mathbf{h}}_i\|^2 \quad (43)$$

for the test dataset, where we denote the  $i$ -th channel realization and corresponding estimate as  $\mathbf{h}_i$  and  $\hat{\mathbf{h}}_i$ , respectively. Accordingly, we define the SNR as

$$\text{SNR} = \frac{E[\|\mathbf{h}\|^2] \|\mathbf{X}\|_F^2}{E[\|\mathbf{n}\|^2]} = \frac{N_{\text{tx}}}{\varsigma^2}. \quad (44)$$

We train the VAEs for a range of SNR values between -19 and 39 dB. Note that the proposed estimators are, therefore, SNR-independent. During the training of VAE-noisy and VAE-real, we sample new realizations  $\mathbf{n}$  after every epoch. We train the VAEs until (37) does not improve for 100 consecutive epochs on the validation dataset.

### A. Training Dataset and Architecture Study

Initially, we investigate two critical quantities of the model selection process: the training dataset's size and the latent space's dimensionality. Regarding the size of the training dataset, a larger size is likely to lead to better estimation results. Fig. 3 provides insights into this matter. We display the estimation results of the test dataset for the three proposed variants of VAE-based estimators depending on the size of the training dataset. The 3GPP SIMO channel model with three propagation clusters and 128 antennas at the receiver is used in Fig. 3. As dotted lines, we display the attained estimation result for the complete training dataset of 180,000 samples. We also show the estimation performance of the genie-cov estimator in blue. It is visible that the most progress is reached from  $10^2$  to  $10^4$  training samples. More than  $10^4$  training samples only lead to minor NMSE improvements for all three types of VAE-based estimators. Thus, the entire training dataset of 180,000 samples results in convergence of the VAE model weights.

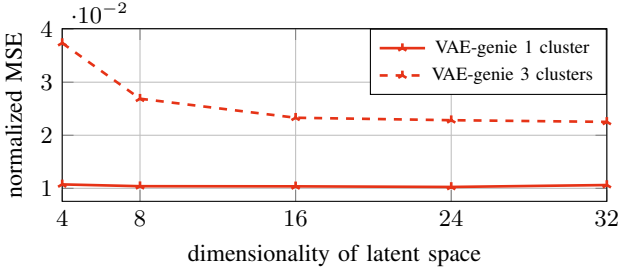


Fig. 4. Normalized MSE for different sizes of the latent space at an SNR of 10 dB for the 3GPP SIMO channel model with one or three propagation clusters and 128 antennas at the receiver.

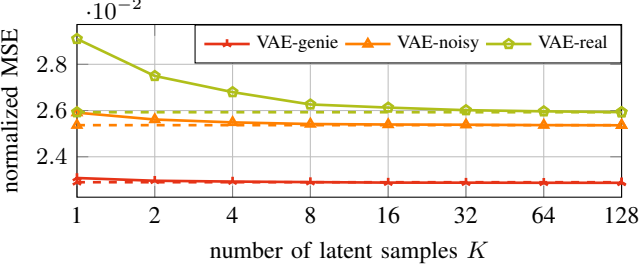


Fig. 5. Normalized MSE for different numbers of samples  $K$  drawn in the latent space for the evaluation of  $\hat{h}_{VAE}^{(K)}(\mathbf{y})$  at an SNR of 10 dB for the 3GPP SIMO channel model with three propagation clusters and 128 antennas at the receiver. The dashed lines represent the estimate  $\hat{h}_{VAE}(\mathbf{y})$  in (25).

The influence of the dimensionality of the latent space on the estimation result is less apparent than the size of the training dataset. The latent vector is an abstract quantity without obvious physical meaning, which makes it intricate to select an appropriate size. We illustrate the NMSE for dimensionalities in the range [4, 32] for the 3GPP SIMO channel model with 128 antennas at the receiver in Fig. 4 by considering one and three propagation clusters. The NMSE is nearly constant for the case with one propagation cluster. In contrast, the NMSE decreases from dimensionality 4 to 16 for the three propagation clusters case and saturates for larger dimensional latent spaces. We want to explain this result with the multipath components (MPCs) in mind that constitute a channel. More MPCs are required to describe a channel with three propagation clusters. If the latent space captures intrinsic information about the channel, it makes sense that three clusters need more dimensionality than one cluster. This result motivates the two options for the latent space dimensionality in Table I. In practice, the operator must select an ample enough latent space to obtain good performance.

As pointed out in Section III-B, we approximate the CME with  $\hat{h}_{VAE}(\mathbf{y})$  by only forwarding the latent mean vector  $\mu_\phi(\mathbf{z})$  as a single sample to approximate the outer expectation in (21). It is interesting to see the NMSE performance for different numbers of  $K$  samples from  $q_\phi(\mathbf{z} \mid \mathbf{y})$  to compute  $\hat{h}_{VAE}^{(K)}(\mathbf{y})$  from (24). Fig. 5 provides such an analysis by showing the NMSE for different numbers of latent samples. As dashed lines, we display  $\hat{h}_{VAE}(\mathbf{y})$ , which only uses the single sample  $\mu_\phi(\mathbf{z})$  for the input of the VAE's decoder. We observe that VAE-real benefits the most from more samples. For VAE-genie and VAE-noisy, there are only slight improvements present. Interestingly, only taking the mean value, representing  $\hat{h}_{VAE}(\mathbf{y})$ , delivers an estimation performance of about  $K = 64$

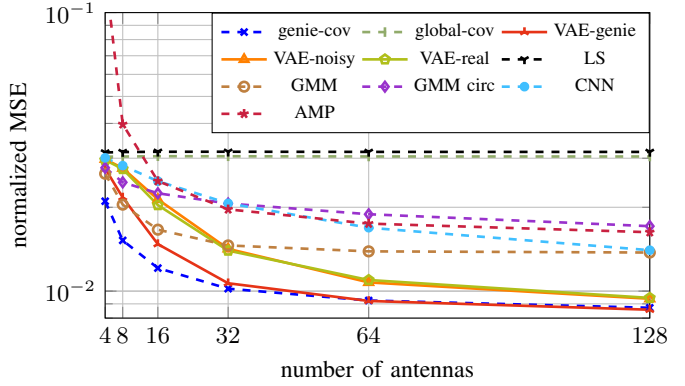


Fig. 6. Normalized MSE for the 3GPP SIMO channel model with three propagation clusters for different numbers of antennas at the receiver at an SNR of 15 dB. The proposed methods are displayed with solid linestyles.

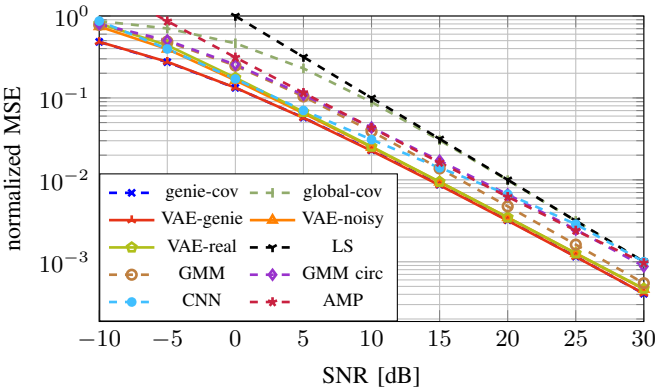


Fig. 7. Normalized MSE for the 3GPP SIMO channel model with three propagation clusters and 128 antennas at the receiver. The proposed methods are displayed with solid linestyles.

latent samples for VAE-real. The excellent performance of  $\hat{h}_{VAE}(\mathbf{y})$  is a supporting argument for the conjecture that the estimator is linear in the vicinity of the latent mean vector as explained in the last paragraph of Section III-B.

### B. SIMO Case

We examine the SIMO case in this section, where every plot relates to the SIMO signal model in (5). We begin with an NMSE investigation for the 3GPP channel model with three propagation clusters and varying numbers of antennas at the receiver at an SNR of 15 dB in Fig. 6. The GMM estimator is also evaluated with a circulant restriction on the covariance matrices of the GMM components, termed GMM circ, cf. [18]. The illustration shows that the proposed VAE-based methods need a sufficiently large amount of antennas to develop their full potential. From 32 antennas on, VAE-noisy and VAE-real outperform the GMM and exhibit increasing performance gains if more antennas are considered. All other baselines perform significantly worse than the proposed methods in the large antenna regime. It is also visible that VAE-genie converges to the genie-cov curve for more than 32 antennas.

A massive amount of antennas is significant for prospective communications systems. Hence, we investigate the large antenna regime in more detail in the following. In Fig. 7, we display the NMSE performance over the SNR for the same

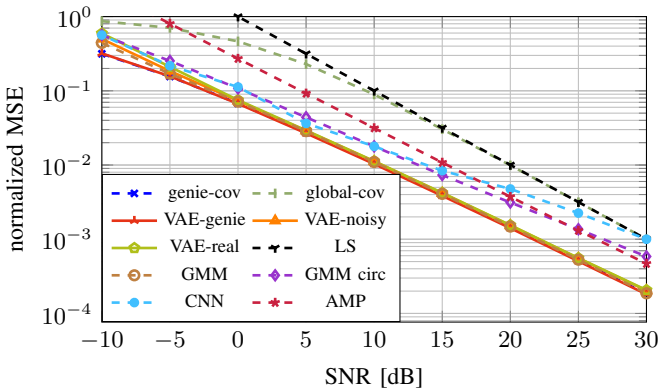


Fig. 8. Normalized MSE for the 3GPP SIMO channel model with one propagation cluster and 128 antennas at the receiver. The proposed methods are displayed with solid linestyles.

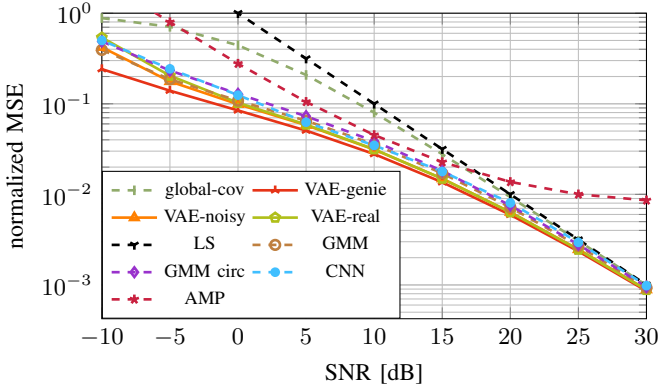


Fig. 9. Normalized MSE for the QuaDRiGa SIMO channel model with LOS channels and 128 antennas at the receiver. The proposed methods are displayed with solid linestyles.

system as in Fig. 6. The overall impression of the behavior in Fig. 7 is similar to Fig. 6. VAE-genie exhibits the best NMSE values and lies almost on top of genie-cov over the whole SNR range. VAE-noisy and VAE-real show better NMSE values than GMM for every SNR instance with a gain between 2 and 3 dB. The performance gains of the proposed methods compared to the remaining baseline estimators are even more significant. For example, at 10 dB, VAE-real has approximately an advantage of 3 and 7 dB compared to the AMP and LS methods, respectively.

We inspect the NMSE performance for the 3GPP channel model with one propagation cluster and 128 antennas at the receiver over the SNR in Fig. 8. The performance advantages of the proposed estimators in terms of the NMSE are more prominent compared to the three clusters case, especially for high SNR. Only GMM shows comparable performance and lies almost on the proposed VAE-based estimators. Only for SNR values below 0 dB, VAE-genie exhibits a slightly lower NMSE. The proposed estimators achieve about 10 dB advantage compared to LS over the whole SNR range.

The 3GPP channel model defines the channel as CG. The QuaDRiGa channel model has no CG assumption, so we show corresponding results in Fig. 9. We display the NMSE performance for a system with one dominant LOS path and 128 antennas at the receiver. This time, we cannot display the genie-cov curve as the true CCM is unavailable. As can

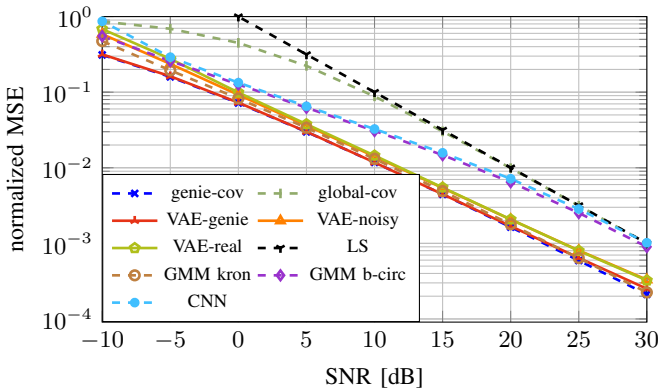


Fig. 10. Normalized MSE for the 3GPP MIMO channel model with one propagation cluster, 32 antennas at the receiver, and 4 antennas at the transmitter. The proposed methods are displayed with solid linestyles.

be seen in the plot, all VAE-based estimators show strong NMSE results. The advantages are not as pronounced as in the previous figures but still noticeable. VAE-genie preserves its status as a benchmark result because it achieves the lowest NMSE for every SNR value.

In summary, the VAE-based methods exhibit high performance gains for large antenna arrays, i.e., larger equal 32 antennas and all considered numbers of propagation clusters. The strong performance for arrays with many antennas is likely due to the circulant approximation to the Toeplitz CCM, which becomes better for more antennas. Moreover, all ML-based methods use genie knowledge during the training phase in the form of noise-free channel training data, except for VAE-real, which is trained and evaluated solely based on noisy pilot observations. In this light, the strong CE results of VAE-real are even more meaningful.

### C. MIMO Case

This section discusses estimation results for the MIMO signal model from (2). We include the GMM-based estimator with Kronecker assumption at the transmitter and receiver (GMM kron), and the GMM with a block-circulant restriction on the fitted CCMs (GMM b-circ), cf. [18]. Note that GMM kron achieves almost identical performance as a GMM without the Kronecker assumption as demonstrated in [18].

Fig. 10 shows the NMSE performance for the 3GPP MIMO channel model with one propagation cluster, 32 antennas at the receiver, and 4 antennas at the transmitter. The qualitative behavior of the curves is similar to Fig. 8, where also one propagation cluster is considered. CNN and GMM b-circ show the worst NMSE among the ML-based methods for SNRs larger than -5 dB. VAE-noisy and VAE-real show comparable performance as GMM kron, with a slight advantage for GMM kron for higher SNRs. Compared to LS, the VAE-based methods attain a performance gain between 6 and 13 dB.

In Fig. 11, we illustrate estimation results for the 3GPP MIMO channel model with three propagation clusters, 32 antennas at the receiver, and 4 antennas at the transmitter. This figure has many attributes in common with Fig. 7. VAE-noisy and VAE-real outperform GMM kron. The performance gain compared to LS shrinks to a range from 2 to 11 dB.

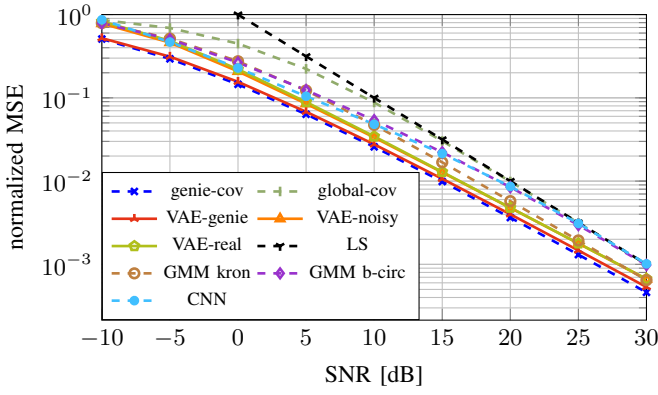


Fig. 11. Normalized MSE for the 3GPP MIMO channel model with three propagation clusters, 32 antennas at the receiver, and 4 antennas at the transmitter. The proposed methods are displayed with solid linestyles.

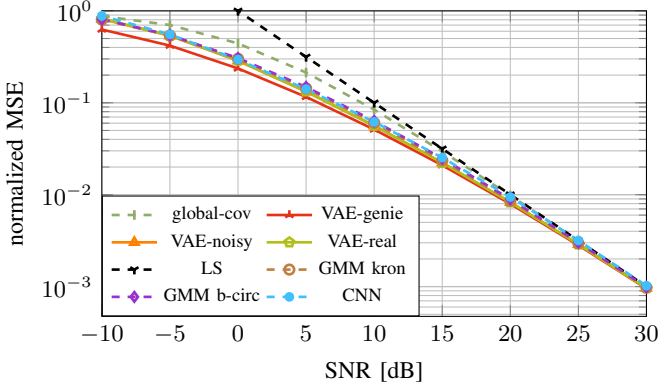


Fig. 12. Normalized MSE for the QuaDRiGa MIMO channel model with mixed NLOS/LOS channels, 32 antennas at the receiver, and 4 antennas at the transmitter. The proposed methods are displayed with solid linestyles.

Fig. 12 presents estimation results for the QuaDRiGa MIMO channel model with mixed NLOS/LOS channels, 32 antennas at the receiver, and 4 antennas at the transmitter. Compared to the previous figures, Fig. 12 shows less prominent NMSE advantages of the proposed estimators. All methods converge to the LS curve for high SNR. Furthermore, all learning-based methods exhibit a resembling performance. Only the VAE-genie variant has a slightly better performance than the baseline estimators.

In a strong NLOS environment with many weak propagation paths, as it is present in Fig. 12, there is less channel structure present in the available training dataset that can be exploited. In contrast, the previous evaluations demonstrated that the proposed estimators exhibit significant performance gains over the baselines in scenarios with fewer propagation paths. These observations are relevant, especially for mmWave or THz communications, since such systems imply few paths, which are ideal conditions for the proposed estimators.

## VII. CONCLUSION

This manuscript presents a novel CE technique based on the generative model VAE. The idea is to model the underlying channel distribution as CG via a VAE. The CG modeling allows us to parameterize the MSE-optimal CME under the VAE framework. We provide theoretical analysis that underpins the strong estimation capabilities of the proposed VAE-based

estimators. We propose three variants of VAE-based estimator, of which we find the VAE-real variant particularly appealing as it does not require access to noise-free channel data, neither during the training nor during the evaluation phase. Our extensive numerical simulations highlight that the proposed methods attain excellent CE performance for various system configurations. In future work, we want to investigate the underdetermined system case with fewer pilots than transmit antennas or a broad matrix  $\mathbf{A}$ , which includes wideband systems. Moreover, we plan to explore more advanced VAE architectures, e.g., by incorporating a NF in the latent space.

## APPENDIX

### A. Proof of Theorem 1

*Proof.* First, we plug in Bayes' theorem in (32), cf. (31), and then find an upper bound in which we can utilize the uniform convergence properties of (29) and (30):

$$\left\| \frac{p_{\theta}^{(\tau)}(\mathbf{h} | \mathbf{z})p(\mathbf{z})}{q_{\phi}^{(\eta)}(\mathbf{z} | \mathbf{h})} - \frac{p(\mathbf{h} | \mathbf{z})p(\mathbf{z})}{p(\mathbf{z} | \mathbf{h})} \right\|_{\infty} \leq \|p(\mathbf{z})\|_{\infty} \left\| \frac{p_{\theta}^{(\tau)}(\mathbf{h} | \mathbf{z})}{q_{\phi}^{(\eta)}(\mathbf{z} | \mathbf{h})} - \frac{p(\mathbf{h} | \mathbf{z})}{p(\mathbf{z} | \mathbf{h})} \right\|_{\infty} \quad (45)$$

$$= \|p(\mathbf{z})\|_{\infty} \left\| \frac{p_{\theta}^{(\tau)}(\mathbf{h} | \mathbf{z})p(\mathbf{z} | \mathbf{h}) - q_{\phi}^{(\eta)}(\mathbf{z} | \mathbf{h})p(\mathbf{h} | \mathbf{z})}{q_{\phi}^{(\eta)}(\mathbf{z} | \mathbf{h})p(\mathbf{z} | \mathbf{h})} \right\|_{\infty} \quad (46)$$

$$\leq \|p(\mathbf{z})\|_{\infty} \frac{\left\| p_{\theta}^{(\tau)}(\mathbf{h} | \mathbf{z}) \left( p(\mathbf{z} | \mathbf{h}) - q_{\phi}^{(\eta)}(\mathbf{z} | \mathbf{h}) \right) \right\|_{\infty}}{\|q_{\phi}^{(\eta)}(\mathbf{z} | \mathbf{h})p(\mathbf{z} | \mathbf{h})\|_{\infty}} + \|p(\mathbf{z})\|_{\infty} \frac{\left\| q_{\phi}^{(\eta)}(\mathbf{z} | \mathbf{h}) \left( p_{\theta}^{(\tau)}(\mathbf{h} | \mathbf{z}) - p(\mathbf{h} | \mathbf{z}) \right) \right\|_{\infty}}{\|q_{\phi}^{(\eta)}(\mathbf{z} | \mathbf{h})p(\mathbf{z} | \mathbf{h})\|_{\infty}} \quad (47)$$

$$\leq \underbrace{\|p(\mathbf{z})\|_{\infty} \left\| p_{\theta}^{(\tau)}(\mathbf{h} | \mathbf{z}) \right\|_{\infty}}_{<\infty} \underbrace{\left\| p(\mathbf{z} | \mathbf{h}) - q_{\phi}^{(\eta)}(\mathbf{z} | \mathbf{h}) \right\|_{\infty}}_{\eta \rightarrow \infty \rightarrow 0} + \underbrace{\|p(\mathbf{z})\|_{\infty} \left\| q_{\phi}^{(\eta)}(\mathbf{z} | \mathbf{h}) \right\|_{\infty}}_{<\infty} \underbrace{\left\| p_{\theta}^{(\tau)}(\mathbf{h} | \mathbf{z}) - p(\mathbf{h} | \mathbf{z}) \right\|_{\infty}}_{\tau \rightarrow \infty \rightarrow 0} \quad (48)$$

where in (45) and (48) the Cauchy–Schwarz inequality is used, and in (47) the Cauchy–Schwarz together with the triangle inequality are used. Since both summands in (48) converge to zero for  $\eta, \tau \rightarrow \infty$  by the definition of (29) and (30), the uniform convergence (32) is shown.  $\square$

## REFERENCES

- [1] M. Baur, B. Fesl, M. Koller, and W. Utschick, “Variational Autoencoder Leveraged MMSE Channel Estimation,” in *56th Asilomar Conf. Signals, Syst., Comput.* Pacific Grove, CA, USA: IEEE, 2022, pp. 527–532.
- [2] F. Rusek *et al.*, “Scaling Up MIMO: Opportunities and Challenges with Very Large Arrays,” *IEEE Signal Process. Mag.*, vol. 30, no. 1, pp. 40–60, 2013.

[3] E. Björnson, L. Sanguinetti, H. Wymeersch, J. Hoydis, and T. L. Marzetta, "Massive MIMO is a Reality—What is Next?: Five Promising Research Directions for Antenna Arrays," *Digit. Signal Process.*, vol. 94, pp. 3–20, 2019.

[4] H. Ye, G. Y. Li, and B. H. Juang, "Power of Deep Learning for Channel Estimation and Signal Detection in OFDM Systems," *IEEE Wirel. Commun. Lett.*, vol. 7, no. 1, pp. 114–117, 2018.

[5] M. Soltani, V. Pourahmadi, A. Mirzaei, and H. Sheikhzadeh, "Deep Learning-Based Channel Estimation," *IEEE Commun. Lett.*, vol. 23, no. 4, pp. 2019–2022, 2019.

[6] H. He, C. K. Wen, S. Jin, and G. Y. Li, "Deep Learning-Based Channel Estimation for Beamspace mmWave Massive MIMO Systems," *IEEE Wirel. Commun. Lett.*, vol. 7, no. 5, pp. 852–855, 2018.

[7] D. Neumann, T. Wiese, and W. Utschick, "Learning The MMSE Channel Estimator," *IEEE Trans. Signal Process.*, vol. 66, no. 11, pp. 2905–2917, 2018.

[8] M. B. Mashhadi and D. Gunduz, "Pruning the Pilots: Deep Learning-Based Pilot Design and Channel Estimation for MIMO-OFDM Systems," *IEEE Trans. Wirel. Commun.*, vol. 20, no. 10, pp. 6315–6328, 2021.

[9] W. Yu, F. Sohrabi, and T. Jiang, "Role of Deep Learning in Wireless Communications," *IEEE BITS Inf. Theory Mag.*, vol. 2, no. 2, pp. 56–72, 2022.

[10] H. He *et al.*, "Model-Driven Deep Learning for Physical Layer Communications," *IEEE Wirel. Commun.*, vol. 26, no. 5, pp. 77–83, 2019.

[11] N. Shlezinger, J. Whang, Y. C. Eldar, and A. G. Dimakis, "Model-Based Deep Learning," *Proc. IEEE*, vol. 111, no. 5, pp. 465–499, 2023.

[12] L. Ruthotto and E. Haber, "An introduction to deep generative modeling," *GAMM-Mitteilungen*, vol. 44, no. 2, p. e202100008, 2021.

[13] C. M. Bishop, *Pattern Recognition and Machine Learning*. Springer, 2006.

[14] D. J. Rezende, S. Mohamed, and D. Wierstra, "Stochastic Backpropagation and Approximate Inference in Deep Generative Models," in *Proc. 31st Int. Conf. Mach. Learn.*, 2014.

[15] D. P. Kingma and M. Welling, "Auto-Encoding Variational Bayes," in *Proc. 2nd Int. Conf. Learn. Represent.*, 2014.

[16] I. Goodfellow *et al.*, "Generative Adversarial Networks," *Commun. ACM*, vol. 63, no. 11, pp. 139–144, 2020.

[17] G. Papamakarios, E. Nalisnick, D. J. Rezende, S. Mohamed, and B. Lakshminarayanan, "Normalizing Flows for Probabilistic Modeling and Inference," *J. Mach. Learn. Res.*, vol. 22, pp. 1–64, 2021.

[18] M. Koller, B. Fesl, N. Turan, and W. Utschick, "An Asymptotically MSE-Optimal Estimator Based on Gaussian Mixture Models," *IEEE Trans. Signal Process.*, vol. 70, pp. 4109–4123, 2022.

[19] E. Balevi and J. G. Andrews, "Wideband Channel Estimation With a Generative Adversarial Network," *IEEE Trans. Wirel. Commun.*, vol. 20, no. 5, pp. 3049–3060, 2021.

[20] E. Balevi, A. Doshi, A. Jalal, A. Dimakis, and J. G. Andrews, "High Dimensional Channel Estimation Using Deep Generative Networks," *IEEE J. Sel. Areas Commun.*, vol. 39, no. 1, pp. 18–30, 2021.

[21] A. Caciularu and D. Burshtein, "Blind Channel Equalization using Variational Autoencoders," in *IEEE Int. Conf. Commun. Work.*, 2018.

[22] —, "Unsupervised Linear and Nonlinear Channel Equalization and Decoding Using Variational Autoencoders," *IEEE Trans. Cogn. Commun. Netw.*, vol. 6, no. 3, pp. 1003–1018, 2020.

[23] V. Lauinger, F. Buchali, and L. Schmalen, "Blind Equalization and Channel Estimation in Coherent Optical Communications Using Variational Autoencoders," *IEEE J. Sel. Areas Commun.*, vol. 40, no. 9, pp. 2529–2539, 2022.

[24] T. Zhao and F. Li, "Variational-autoencoder signal detection for MIMO-OFDM-IM," *Digit. Signal Process.*, vol. 118, p. 103230, 2021.

[25] T. Zhao, F. Li, and P. Tian, "A Deep-Learning Method for Device Activity Detection in mMTC under Imperfect CSI Based on Variational-Autoencoder," *IEEE Trans. Veh. Technol.*, vol. 69, no. 7, pp. 7981–7986, 2020.

[26] W. Xia *et al.*, "Generative Neural Network Channel Modeling for Millimeter-Wave UAV Communication," *IEEE Trans. Wirel. Commun.*, vol. 21, no. 11, pp. 9417–9431, 2022.

[27] B. Fesl *et al.*, "Channel Estimation based on Gaussian Mixture Models with Structured Covariances," in *2022 56th Asilomar Conf. Signals, Syst. Comput.* Pacific Grove, CA, USA: IEEE, 2022, pp. 533–537.

[28] B. Fesl, N. Turan, M. Joham, and W. Utschick, "Learning a Gaussian Mixture Model from Imperfect Training Data for Robust Channel Estimation," *IEEE Wirel. Commun. Lett.*, vol. 12, no. 3, pp. 1066–1070, 2023.

[29] R. M. Gray, "Toeplitz and Circulant Matrices: A Review," *Found. and Trends® in Commun. and Inf. Theory*, no. 3, pp. 155–239, 2006.

[30] 3GPP, "Spatial channel model for Multiple Input Multiple Output (MIMO) simulations (Release 16)," 3rd Generation Partnership Project (3GPP), Tech. Rep. 25.996 V16.0.0, 2020.

[31] J. Kermoal, L. Schumacher, K. Pedersen, P. Mogensen, and F. Frederiksen, "A Stochastic MIMO Radio Channel Model With Experimental Validation," *IEEE J. Sel. Areas Commun.*, vol. 20, no. 6, pp. 1211–1226, 2002.

[32] S. Jaeckel, L. Raschkowski, K. Borner, and L. Thiele, "QuaDRiGa: A 3-D Multi-Cell Channel Model With Time Evolution for Enabling Virtual Field Trials," *IEEE Trans. Antennas Propag.*, vol. 62, no. 6, pp. 3242–3256, 2014.

[33] S. Jaeckel *et al.*, "QuaDRiGa - Quasi Deterministic Radio Channel Generator, User Manual and Documentation," Fraunhofer Heinrich Hertz Institute, Tech. Rep. v2.6.1, 2021.

[34] S. M. Kay, *Fundamentals of Statistical Signal Processing: Estimation Theory*. Englewood Cliffs, NJ: Prentice-Hall, Inc., 1993.

[35] A. Banerjee, X. Guo, and H. Wang, "On the Optimality of Conditional Expectation as a Bregman Predictor," *IEEE Trans. Inf. Theory*, vol. 51, no. 7, pp. 2664–2669, 2005.

[36] D. M. Blei, A. Kucukelbir, and J. D. McAuliffe, "Variational Inference: A Review for Statisticians," *J. Am. Stat. Assoc.*, vol. 112, no. 518, pp. 859–877, 2017.

[37] M. Loève, *Probability Theory I*, 4th ed. Springer New York, NY, 1977.

[38] S. Park, C. Yun, J. Lee, and J. Shin, "Minimum width for universal approximation," in *Int. Conf. Learn. Represent.*, 2021.

[39] P. Kidger and T. Lyons, "Universal approximation with deep narrow networks," in *Proc. Conf. Learn. Theory*, vol. 125, 2020, pp. 2306–2327.

[40] D. P. Kingma and M. Welling, "An Introduction to Variational Autoencoders," *Found. Trends® Mach. Learn.*, vol. 12, no. 4, pp. 307–392, 2019.

[41] J. Bergstra and Y. Bengio, "Random Search for Hyper-Parameter Optimization," *J. Mach. Learn. Res.*, vol. 13, no. 10, pp. 281–305, 2012.

[42] R. Liaw *et al.*, "Tune: A Research Platform for Distributed Model Selection and Training," *arXiv preprint arXiv:1807.05118*, 2018.

[43] S. Ioffe and C. Szegedy, "Batch Normalization: Accelerating Deep Network Training by Reducing Internal Covariate Shift," in *Proc. 32nd Int. Conf. Mach. Learn.*, Lille, 2015, pp. 448–456.

[44] T. Salimans and D. P. Kingma, "Weight Normalization: A Simple Reparameterization to Accelerate Training of Deep Neural Networks," *30th Conf. Neural Inf. Process. Syst.*, 2016.

[45] J. L. Ba, J. R. Kiros, and G. E. Hinton, "Layer Normalization," in *Adv. Neural Inf. Process. Syst. - Deep Learn. Symp.*, 2016.

[46] S. Anwar, K. Hwang, and W. Sung, "Structured Pruning of Deep Convolutional Neural Networks," *ACM J. Emerg. Technol. Comput. Syst.*, vol. 13, no. 3, pp. 1–18, 2017.

[47] S. A. Busari, K. M. S. Huq, S. Mumtaz, L. Dai, and J. Rodriguez, "Millimeter-Wave Massive MIMO Communication for Future Wireless Systems: A Survey," *IEEE Commun. Surv. Tutorials*, vol. 20, no. 2, pp. 836–869, 2018.

[48] D. L. Donoho, A. Maleki, and A. Montanari, "Message passing algorithms for compressed sensing: I. motivation and construction," in *2010 IEEE Inf. Theory Work. Inf. Theory*. IEEE, 2010, pp. 1–5.

[49] A. Maleki, L. Anitori, Z. Yang, and R. G. Baraniuk, "Asymptotic Analysis of Complex LASSO via Complex Approximate Message Passing (CAMP)," *IEEE Trans. Inf. Theory*, vol. 59, no. 7, pp. 4290–4308, 2013.

[50] B. Fesl, N. Turan, M. Koller, and W. Utschick, "A Low-Complexity MIMO Channel Estimator with Implicit Structure of a Convolutional Neural Network," in *22nd Int. Work. Signal Process. Adv. Wirel. Commun.* IEEE, 2021, pp. 11–15.